ACS APPLIED MATERIALS & INTERFACES

Research Article

Cite This: ACS Appl. Mater. Interfaces 2018, 10, 23573−23582

www.acsami.org

Melanin Nanoparticle-Incorporated Silk Fibroin Hydrogels for the Enhancement of Printing Resolution in 3D-Projection Stereolithography of Poly(ethylene glycol)-Tetraacrylate Bio-ink

Sungchul Shin,[†] Hojung Kwak,[†] and Jinho Hyun*[,†,‡,§]

[†]Department of Biosystems and Biomaterials Science and Engineering, Seoul National University, Seoul 151-921, Republic of Korea

[‡]Research Institute of Agriculture and Life Sciences, Seoul National University, Seoul 151-921, Republic of Korea

[§]Center for Food and Bioconvergence, Seoul National University, Seoul 151-921, Republic of Korea

Supporting Information

ABSTRACT: It is not easy to design structures with transparent solutions, especially in light projection three-dimensional (3D) printing, since the penetration of light in solution is limitless. Here, silk fibroin incorporated with melanin nanoparticles (SFM) is used as a transparency modifier of poly(ethylene glycol)-tetraacrylate (PEG4A) solution. The incorporation of melanin into the SF hydrogel is performed in the range of 0.05−0.2% (w/v), and the SFM was added to the PEG4A precursor solution at 0.25−1.0% (w/v). The printing accuracy was examined by comparing the printed and designed feature sizes. The addition of 1.0% (w/v) SFM to a 4% (w/v) PEG4A (PEG4A/SFM) precursor solution effectively reduces the transparency of the solution and improves the printing resolution by confining the light beam to a designed region. This enables the fabrication of hard-to-express features such as hollow blood vessels or vacant tubes. Furthermore, the elastic modulus of the printed PEG4A/SFM composite hydrogel increases 2.5-fold higher than the PEG4A hydrogel without SFM. For the bio-ink, PEG4A/SFM-containing cells show non-cytotoxicity and improve the proliferation rate of embedded cells, confirming the high biocompatibility of PEG4A/SFM hydrogels.

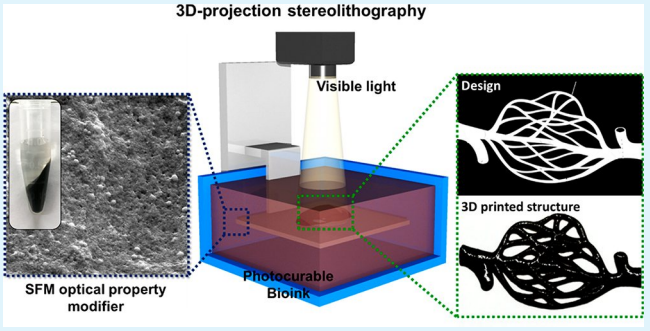

KEYWORDS: *silk fibroin, melanin nanoparticle, PEG tetraacrylate, digital light process (DLP), 3D printing resolution, bio-ink*

1. INTRODUCTION

Currently, three-dimensional (3D) printing techniques are well-established for the fabrication of complicated structures such as bones, teeth, or organ replicas and considered as a key technology for implementing complex cardiovascular structures.[1,2] In recent time, the controllable fabrication of cell-laden hydrogel structures has become more important in tissue engineering, pharmaceutical, and cosmetic industries due to international restriction of animal examinations. However, 3D printing ink materials that are photo-cross-linkable in a visible range of light are rarely reported, especially for the formation of cell-laden structures.

To fabricate cell-laden hydrogel constructs, the materials constituting the bio-inks are biocompatible, so that the embedded cells can survive and proliferate properly.[3−6] In addition, the designed features must be printed precisely at high resolution.[7,8] The biocompatible materials, including polypeptides, carbohydrate polymers, and synthetic polymers, have been challenged as a photo-cross-linkable precursor solution by modifying with acryl groups. The structuring of these materials is mainly available through direct ink-writing 3D printing.[9−11] However, this printing is not appropriate for structures requiring high printing resolution, due to the limit of selectable extrusion nozzles and the development of roughness due to additive manufacturing.

Three-dimensional projection stereolithography (SLA) is increasingly used for the fabrication of biomimetic complex scaffolds and hydrogels for tissue engineering and pharmaceutics. Compared with laser-based SLA techniques, digital light process (DLP) 3D printing is particularly suitable for the 3D fabrication of cell-laden hydrogels, due to the shorter production time and the use of visible light rather than ultraviolet light.[12−14]

Acrylate modified polymeric materials have been developed for SLA and DLP 3D printing.[5,12−15] However, the printing resolution on the *z*-axis cannot be controlled, because the acrylate-modified polymeric materials are transparent.[16] The printing resolution on the *z*-axis is dependent on the penetration depth of light through the inks. Thus, the transparency of the inks should be controlled by the addition of colored biomaterials to the inks.

Received: April 13, 2018
Accepted: June 25, 2018
Published: June 25, 2018

DOI: 10.1021/acsami.8b05963
ACS Appl. Mater. Interfaces 2018, 10, 23573−23582

Biologically derived melanin nanoparticles were chosen as a functional pigment of composite bio-inks because of their uniformity in shape and size, high light absorption, high biocompatibility, chemical inertness, and availability of mass production.[17,18] Melanin nanoparticles are membrane-bound granules whose size is up to 500 nm in diameter. They are believed to template the polymerization of melanin, and their shape is very uniform and consistent for a given species and their maturity. Melanin nanoparticles are typically a rounded complex covered by a bilipid membrane, which is a main component of living organisms. Such a unique structure of melanin nanoparticles enhances the biocompatibility and the inertness to nearby molecules compared with a low molecular weight of organic or inorganic dyes and pigments. In addition, the black-colored melanin nanoparticles were more efficient in the light absorption compared with the other colored pigments. Inorganic pigments are well-developed, but their biocompatibility was not established in biological and medical applications because they are mostly composed of metal complexes.

Polymeric hydrogels are incorporated with a variety of additive materials including carbon-based particles,[19,20] functional polymers,[21,22] inorganic/ceramic compounds,[23−25] and metal/metal oxide complexes[26,27] for the development of advanced biomaterials in tissue engineering. Especially, the cell-laden hydrogels need to incorporate with functional materials to ensure the cell viability and metabolic activity.

Silk fibroin (SF)-based materials have been widely applied in tissue engineering because of their excellent biocompatibility, degradability, and bioactivity.[28−30] In addition, the facile processability and reinforcing capability of SF hydrogel in the hybrid structures are considered a generic component of biocomposite materials.[30−34] In the research, SF incorporated with melanin nanoparticles (SFM) was chosen as a biocompatible colored additive to the transparent ink. The constituents of SFM were tailored to exhibit the desired optical properties required to achieve the high resolution geometries throughout 3D-projection stereolithography. Furthermore, artificial vascular-like structures were printed with SFM-containing bio-ink and the perfusion experiment was performed to verify the reliable continuous flow of fluids without leaking. SFM has excellent biocompatibility, improves the printing accuracy efficiently, and can be a generic material as an optical property modifier of transparent bio-inks in stereolithography.

2. EXPERIMENTAL SECTION

2.1. Preparation of SFM Additives. The SF aqueous solution was prepared according to the method reported by Kaplan et al.[35] *Bombyx mori* silk cocoons were degummed by boiling twice for 1 h each in a water solution of 3 g of sodium oleate and 2 g of sodium carbonate to remove sericin. Degummed silk was then washed several times in distilled water (DI water) and dried at 60 °C in an oven for 1 day. The obtained SF was dissolved in a 9.3 M lithium bromide aqueous solution (Kanto Chemical, Japan) at 60 °C for 1 h. The SF solution was dialyzed against distilled water to remove lithium bromide using a cellulose acetate membrane (MWCO, 12−14 kDa). To induce the gelation of the SF solution, a 1% of SF solution was tip-sonicated for 10 min at 50% amplitude.[36,37]

The melanin nanoparticles were extracted from cuttlefish ink (Nortindal Sea Products, Spain). Viscose cuttlefish ink (70% ink, 20% DI water, 9% sodium chloride, and 1% sodium carboxymethyl cellulose) was diluted to 7% ink concentration and dialyzed against DI water to remove sodium chloride using a cellulose acetate membrane (MWCO, 12−14 kDa) at 60 °C for 7 days.

To prepare the SFM, the SF hydrogel was mixed with melanin nanoparticles in various concentrations. Then, the mixture was autoclaved at 120 °C for 20 min to induce the adsorption of melanin nanoparticles on the surface of the SF hydrogel. After centrifugation at 3000 rpm for 5 min, the supernatant was removed from the tube and resuspended with DI water.

2.2. Preparation of Visible Light Cross-Linkable Precursor Solution. The four-arm PEG-hydroxyl (20 kDa, PEG−OH) reagent was obtained from JenKem Technology USA. Eosin-Y disodium salt, triethanolamine (TEA), and *N*-vinylpyrrolidone (NVP) were purchased from Sigma-Aldrich (St. Louis, MO, USA). For the synthesis of PEG4A, 5 g of PEG−OH was dissolved in 100 mL of anhydrous toluene and heated to 130 °C to remove excess water. Then, toluene in the solution was completely removed using a rotary evaporator, and the bottle containing PEG−OH was cooled to room temperature. The PEG−OH in the bottle was dissolved again with 50 mL of dichloromethane. Acryloyl chloride (3 equiv of OH group on PEG) and triethylamine (3 equiv) were added slowly to the PEG−OH solution through an addition funnel and vigorously stirred for 30 min in an ice bath. The reaction was allowed to proceed overnight at room temperature in the dark. The solution was filtered through a thin layer of Hyflo, followed by precipitation in cold ethyl ether. The precipitated PEG-tetraacrylate (PEG4A) was collected and dried under vacuum overnight in the dark, redissolved in deionized water, and dialyzed in a 3.5 kDa MWCO dialysis tube for 3 days. To prepare the bio-ink precursor solution, the prepared SFM in various adsorption concentrations was mixed with the synthesized 4% (w/v) PEG4A. Eosin-Y (0.1 mM), TEA (0.3%), and NVP (0.3%) were added to the precursor solution for visible light cross-linking of the bio-ink.

2.3. Measurement of Turbidity in Precursor Solutions. The turbidity of the PEG4A precursor solution containing 0, 0.25, 0.5, 0.75, and 1.0% (w/v) of SFM was measured using a microplate reader (Synergy HT, BioTek, Winooski, VT, USA) at 550 nm. Then, 50 μL of the precursor solutions were loaded into a 96-well plate, and the average absorbance value was obtained.

2.4. Visible Light-Induced 3D Printing. During printing, the displayed pattern from a projector (Vivitek, USA) was controlled with a computer via the HDMI port. The patterns were designed using the commercially available Rhinoceros software (Rhinoceros 5.0, Robert McNeel & Associates, Seattle, WA, USA), with the slices of layers converted to binary color patterns using the slicer software (XMaker, Yinzhou District, Ningbo, Zhejiang, China). The exposed areas were projected in white, while the remaining areas were projected in black. The assigned slices were projected onto the precursor solution through a projector layer-by-layer to generate the hydrogel pattern. A 5 mL aliquot of the hydrogel precursor solution was poured into a 35 × 10 mm^2 Petri dish, and the printing stage was settled at the initiating position inside the precursor solution. A light beam was irradiated on the precursor solution at the printing stage surface for 120 s, and the stage was lowered 2000 μm and maintained for 2 s for complete coverage of the precursor solution on the surface of the layer formed in the previous step. Subsequently, the stage was raised 1750 μm to form a 250 μm thick precursor solution layer for the next hydrogel layer. The repetitive process was performed for cross-linking and accumulating the layers, as designed. In order to print a mesh-type scaffold structure, a structure in which even-numbered layers and odd-numbered layers are orthogonally stacked. In addition, the complex vascular structure was designed to produce a blood vessel structure with an internal cavity. A blood vessel model (diameter, 400 μm) was fabricated to observe the fluid flow in the channel. A solution containing 0.1% (w/v) fluorescent particles was flowed inside the channel, and the flow field was visualized with PIV (particle image velocimetry). The fluid was injected at the different flow rates of 1, 2, and 4 mL/h using a syringe pump, and the images were captured at 10 frames/s using a fluorescence microscope. A Gaussian filter was applied to each image, and the average background noise was subtracted from the images. The velocity vectors were obtained by

DOI: 10.1021/acsami.8b05963
ACS Appl. Mater. Interfaces 2018, 10, 23573−23582

applying 2D cross-correlations of the interrogation windows of 128 × 128 pixels with 50% overlap for the coarse grid and 64 × 64 pixels with 50% overlap for the refined grid system. All image processing procedures were performed in Matlab.

2.6. Evaluation of Printing Accuracy. To evaluate the printing accuracy on the *x*- and *y*-axes, 4% (w/v) PEG4A precursor solutions containing 0.25, 0.5, 0.75, and 1.0% (w/v) SFM were 3D-printed at a different size. The 3D-printed structures were imaged with optical microscopy (Olympus BX51, Tokyo, Japan) and compared to the designed dimensions of structures. To evaluate the printing depth on the *z*-axis, the square feature of the projector light beam (1 cm × 1 cm) was irradiated onto the precursor solutions filling the Petri dish at a 1 cm height for 2 min, and the thickness of the printed hydrogel was measured.

2.7. Rheological Measurements of Bio-inks and Shear Modulus of 3D-Printed Hydrogels. Bio-ink precursor solutions were prepared by mixing 4% (w/v) of PEG4A and variable concentrations of SFM (up to 1.5% (w/v)). The rheological behavior of the bio-inks was analyzed using a digital rheometer (MARS III, Thermo Scientific, Newington, NH, USA) fitted with parallel plate geometry (35 mm radius). To study the shear viscosity of the bio-inks, 1.0 mL of PEG4A/SFM was poured into the geometry at 25 °C, and the measurement was performed in Rot Ramp mode (shear rates, 0.01−1000 s^{-1} with a gap size 1.0 mm). To identify the linear viscoelastic region, the samples were subjected to stress sweep experiments at 25 °C employing a stress range from 0.1 to 100 Pa and a frequency of 1 Hz (see the Supporting Information Figure S1). In situ photorheometry was conducted using a digital rheometer (oscillation time-sweep mode; frequency, 1 Hz; gap size, 80 μm) to observe the gelation behavior. A 50 μL aliquot of the prepolymer solution was placed on the quartz plate of a cure cell and irradiated with visible light via a liquid light guide at room temperature (see the Supporting Information Figure S2). The viscoelastic properties of the printed hydrogels were measured using the digital rheometer. Solutions of 4% (w/v) PEG4A containing variable concentrations of SFM were prepared by dissolving the polymers in a 3T3 cell culture medium. A composite bio-ink was injected into a Petri dish and 3D-printed into the cylindrical structure, which has an 8 mm diameter and 2 mm height. The oscillatory rheometry in the shear strain−sweep mode was performed with a 1 Hz frequency. The gel moduli were measured using parallel plate geometry (8 mm) with a nominal force of 0.2 N and a gap size of 2 mm.

2.8. Cytotoxicity of Composite Hydrogels. NIH 3T3 cells (1.5 × 10^6 cells/mL) were added to three precursor solutions of pure PEG4A, PEG4A containing 1% (w/v) SF, and PEG4A containing 1% (w/v) SFM (0.2% melanin) for the preparation of bio-ink. The bio-inks were 3D-printed with a visible range of light beam for 120 s each layer to form an 8 mm diameter and 2 mm high cylindrical feature shape. After printing with bio-inks, the produced structures were cultured in medium consisting of DMEM with 4.5 g/L glucose, L-glutamine, sodium pyruvate, and 10% FBS. The cells encapsulated in the composite hydrogels were cultured in a humidified 5% CO_2 incubator at 37 °C for 1, 4, 7, 10, and 13 days. To investigate the viability of the encapsulated cells, a live and dead viability/cytotoxicity kit (Invitrogen, Waltham, MA, USA) was used. The live and dead assay reagents were added to a Petri dish containing cell-laden constructs and incubated for 1 h at room temperature in the dark. The fluorescence images of the cell-laden structures were collected using confocal laser scanning microscopy (Carl Zeiss, Germany). For the investigation of cell proliferation, the printed constructs were washed once with PBS and incubated with alamarBlue (Invitrogen) solution for 4 h at 37 °C. The alamarBlue fluorescence was assayed at 540 nm (excitation) and 590 nm (emission) using a microplate reader (Synergy HT, BioTek). The sedimentation of cells was evaluated by the sectional fluorescence images of 3D-printed hydrogel. First, NIH 3T3 cells were labeled with calcein AM fluorescence dye and mixed with a PEG4A precursor solution containing no SFM and the precursor solution containing 1% (w/v) of SFM each in a final concentration of 1.5 × 10^6 cells/mL. Fluorescence images were obtained at 100 μm intervals from the bottom of the hydrogel to confirm the cell dispersion (see the Supporting Information Figure S3).

3. RESULTS AND DISCUSSION

Light-assisted bioprinting platforms are increasingly used for cell printing and tissue engineering applications. These systems mostly involve the photo-cross-linking of biomaterials, which are curable in the visible range of light to maintain cell viability during printing. Here, the 3D printing of a cell-embedding hydrogel was achieved by irradiating the visible range of light onto a photosensitive PEG4A precursor solution with SFM additives using a customized stereolithography projection printer (Figure 1a). The printer was equipped with a DLP

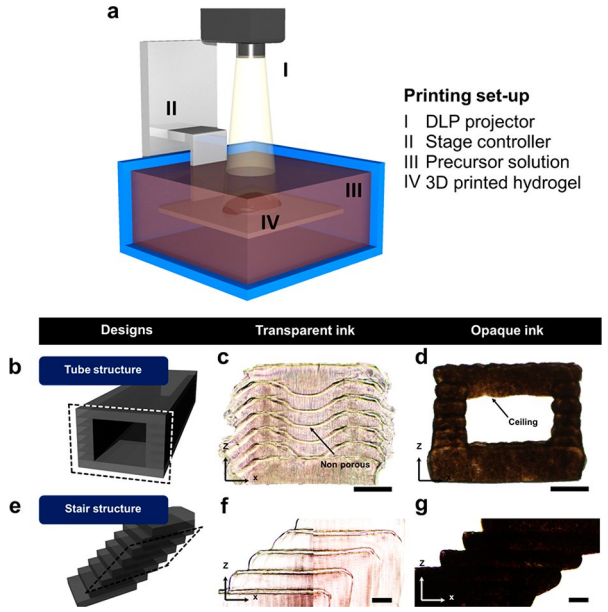

Figure 1. 3D projection stereolithography with SFM embedded bio-ink. (a) Schematic illustration of 3D projection stereolithography. (b) Design of hollow structure. Optical microscopic images of hydrogel cross-section with a tube design using PEG4A-based transparent ink (c) and PEG4A opaque ink containing SFM (d). (e) Design of stair structure. Optical microscopic images of 3D-printed hydrogel cross-section, intended to print stair structures using PEG4A-based transparent ink (f) and PEG4A opaque ink containing SFM (g). Scale bars are 500 μm in panels c, d, f, and g.

projector and a digital micromirror device. The stage controller allowed the precise control of the printing stage at the micrometer scale. The stage immersed in the precursor solution was moved vertically, and layer-by-layer stacking of the hydrogel was achieved.

In stereolithography projection printing, transparent photo-cross-linkable inks can effectively reduce the running time and increase the cross-linking density of the printed features. However, the transparency of the inks diminishes the printing resolution, especially on the *z*-axis due to the undefined penetration depth. For this reason, it is impossible to fabricate empty or tilted structures such as tubes or stairs (Figure 1b,e). In the research, PEG4A was chosen for its high biocompatibility and rapid photo-cross-linking capability, but it is necessary to adjust the transparency to achieve the proper printing resolution. In a simple manner, the lowest level of the layers and the sidewalls were fabricated properly in the 3D printing of the hollow structure using the transparent PEG4A

DOI: 10.1021/acsami.8b05963
ACS Appl. Mater. Interfaces 2018, 10, 23573−23582

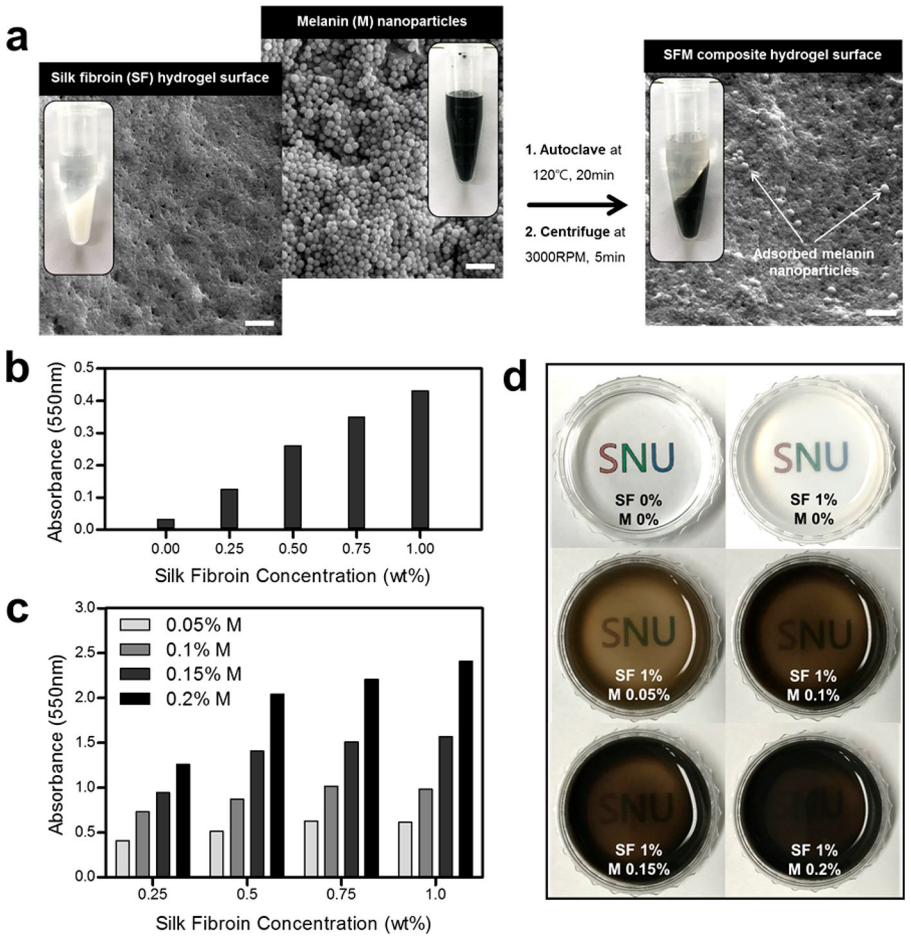

Figure 2. Turbidity of PEG4A/SFM precursor solutions. (a) SEM images of SF hydrogels, melanin nanoparticles, and SFM composite hydrogels. Photographs were taken after centrifuging at 3000 rpm. (b) Turbidity of PEG4A/SF as a function of SF concentration. (c) Turbidity of PEG4A/SFM as a function of SF and melanin concentrations. (d) Photographs of PEG4A/SFM with different concentrations of melanin. PEG4A concentration was 4 wt %. Scale bars are 500 nm in panel a.

bio-ink. However, the light penetrated all layers, from the top ceiling layer to the lowest bottom layer, forming a filled structure despite the design of structures such as tubes or stairs (Figure 1c,f). To enhance the printing resolution in three dimensions, the light absorbance of the ink solution must be controlled and the light beam confined to a certain thickness by controlling the light penetration depth of the ink (Figure 1d,g).

The biocompatibility of bio-inks requires study of critical issues such as the viability and proliferation of cells. SF is well-known as a biocompatible material, and SF hydrogels are easily performed using ultrasonication and homogenization. Here, SFMs were proposed as an additive for the high-resolution 3D printing of biocompatible ink materials. Black melanin nanoparticles were obtained from nature and bound to the SF hydrogel surface without adhesive. The size distribution of melanin nanoparticles was very narrow, and 120 nm of particles were obtained as shown in Figure 2a. The fabrication of biocompatible composite ink materials was achieved in two simple steps. First, the SF aqueous solution was physically cross-linked to SF hydrogels by ultrasonication. Second, the purified melanin nanoparticles were added to the SF hydrogel and heat-treated for the adsorption of melanin nanoparticles to the surface of the SF hydrogel. The incorporation of melanin nanoparticles was confirmed by observing spherical melanin particles at the surface of the SF hydrogel, collected by ultracentrifuge (Figure 2a).

The light absorbance of SF suspension in DI water increased due to light scattering by the SF hydrogels (Figure 2b). Because light scattering can deteriorate the planar printing resolution, it must be suppressed by increased light absorption at the surface of the SF hydrogels. The black melanin was capable of light absorption, and the SFMs were challenged as a potential scattering suppressor for DLP 3D printing. SFM additives with different light absorbance were prepared using a different combination of SF and melanin concentrations. The light absorbance of SFM increased as the concentration of melanin increased. It also increased as the concentration of SF increased due to the increase of the total adsorptive area (Figure 2c). It was determined that melanin adsorption over 95% was achieved with 1.0 wt % SF by measuring the light absorbance of the supernatant solution after ultracentrifugation.

Since the PEG4A precursor solution was highly transparent, it was impossible to print a feature layer-by-layer due to the long penetration depth of light. The addition of 1% (w/v) SF hydrogels without melanin reduced the transparency of the PEG4A precursor solution but resulted in light scattering in the presence of SF hydrogels. Meanwhile, the addition of 1% (w/v) SFM reduced the transparency of PEG4A due to the light absorbance by melanin despite having the same

DOI: 10.1021/acsami.8b05963
ACS Appl. Mater. Interfaces 2018, 10, 23573−23582

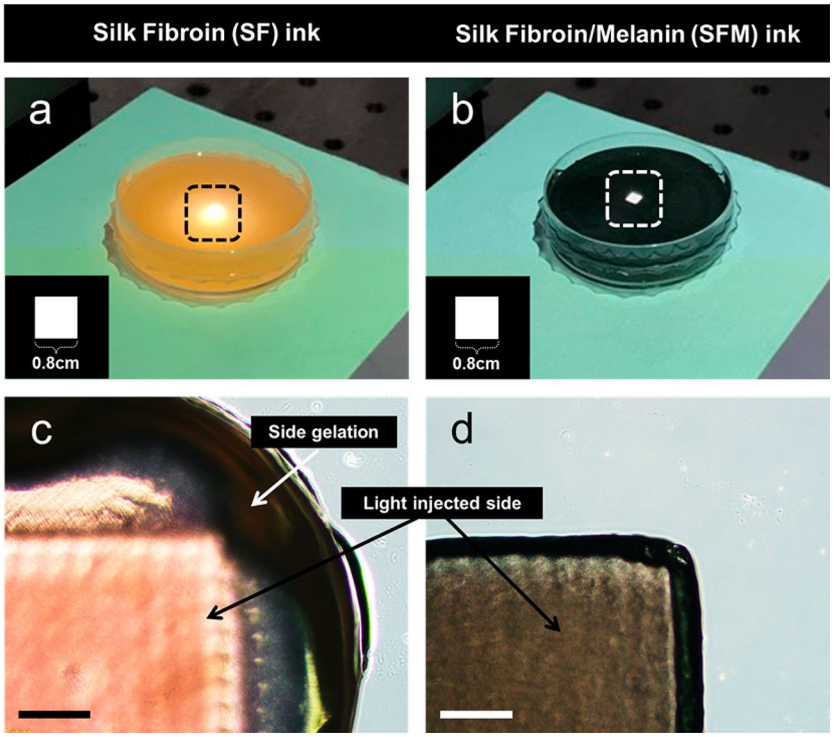

Figure 3. Inhibition of diffusive light scattering of PEG4A precursor solution with SFM. Photographs of square feature (0.8×0.8 cm^2) irradiated in (a) PEG4A/SF and (b) PEG4A/SFM precursor solutions. Optical microscopic images of 3D-printed hydrogels using (c) PEG4A/SF and (d) PEG4A/SFM precursor solutions.

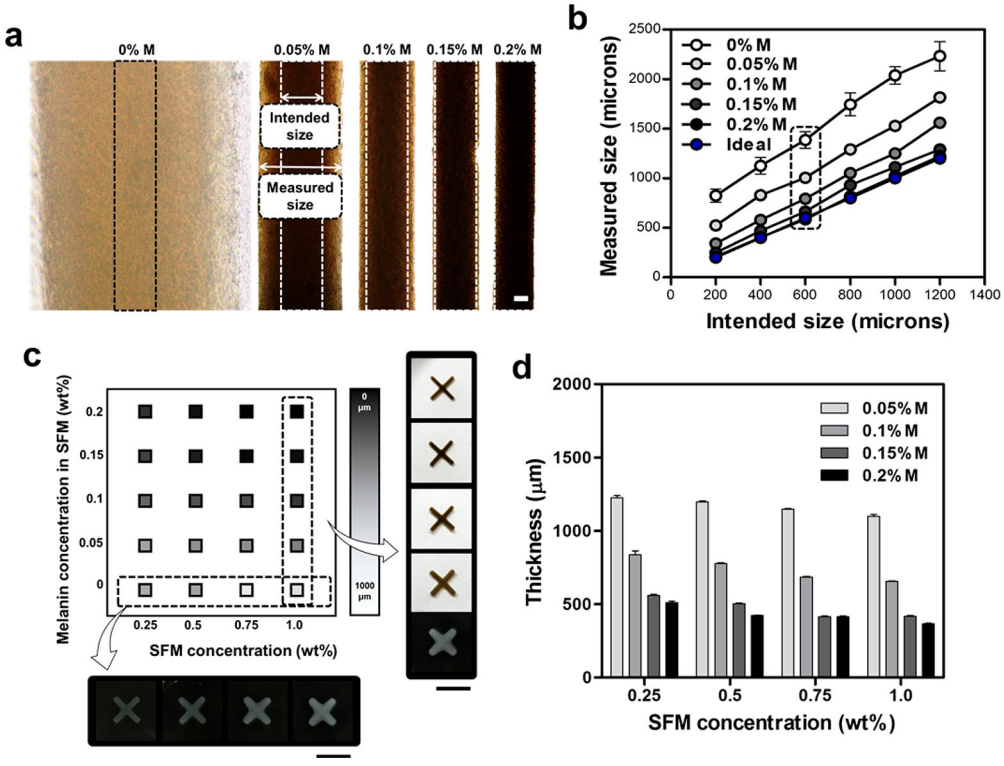

Figure 4. Enhancement of printing resolution with SFM. (a) Optical microscopic images of hydrogels 3D-printed with PEG4A/SFM with varying concentrations of melanin. The concentration of SFM was 1 wt %, and the beam irradiation width was 600 μm. (b) Difference between intended size and measured size of 3D-printed hydrogels at different concentrations of melanin. (c) Mapping of planar resolution with various combinations of SFM and melanin concentrations. Photographs of 3D-printed hydrogels with series of SFM and melanin concentrations. (d) Thickness of hydrogels cross-linked with a precursor solution filled at 1 cm depth. Scale bars are 200 μm in panel a and 1 cm in panel c.

DOI: 10.1021/acsami.8b05963
ACS Appl. Mater. Interfaces 2018, 10, 23573−23582

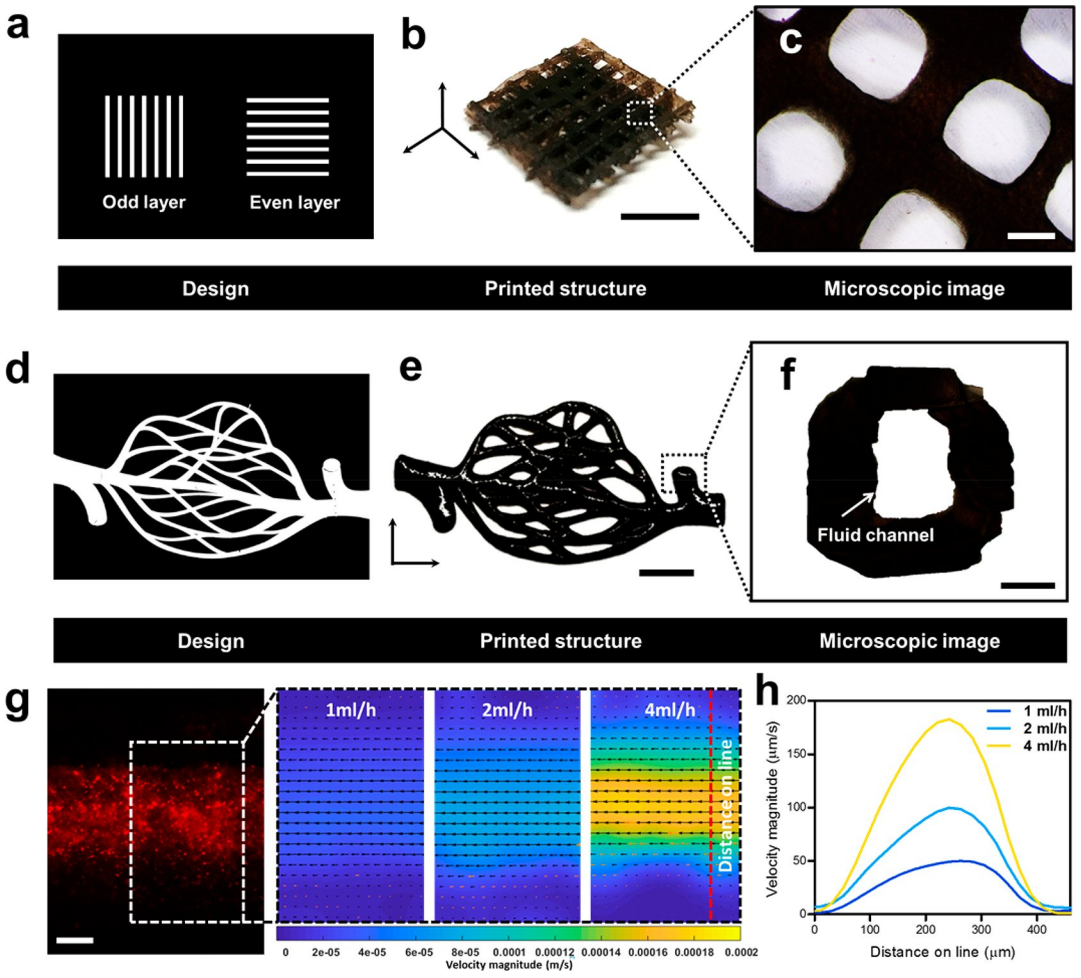

Figure 5. 3D printing of PEG4A/SFM. (a) Design for macroporous meshed structure. (b) Photograph of hydrogel structure 3D-printed using digital beam patterns in panel a. (c) Porous structure of printed hydrogel. (d) Design for a complex blood vessel structure. (e) Photograph of hydrogel structure 3D-printed using digital beam patterns in (d). (f) Cross-sectional view of the hollow structure. (g) Velocity magnitude fields according to the external injection rate in artificial blood vessel model. (h) Velocity profiles according to the external injection rate in artificial blood vessel model. Scale bars are 0.5 cm in panels b and e, 500 μm in panels c and f, and 100 μm in panel g.

concentration as SF (Figure 2d). As the amount of SFM increased in the PEG4A/SFM precursor solution, the light absorbance increased and its color darkened.

The cell-free hydrogel precursor solutions PEG4A/SF and PEG4A/SFM were 3D-printed using visible light projection in a layer-by-layer manner to investigate the printing resolution. The square feature (0.8 × 0.8 cm^2) printed with PEG4A/SF showed a broad range of side gelation, which resulted from the diffusive light scattering of SF hydrogels in the solution, as shown in Figure 3a,c. In contrast, the black SFMs inhibited light diffusion and showed a distinctive edge with square features and low size deviation (Figure 3b,d).

The rheological properties of PEG4A precursor solution containing SFM at 0.5, 1.0, and 1.5% (w/v) were investigated to verify the effect of SFM addition on the viscosity. It was confirmed that the viscosity of the bio-ink was increased as the amount of SFM increased (Figure S1a). In addition, as the SFM concentration increased, the shear stress regions at which the storage modulus was larger than the loss modulus expanded (Figure S1b). However, the addition of SFM above 1.5% (w/v) induced the formation of a concave structure on the upper surface of the object because the fluidity of the solution for the next layer decreased (Figure S1c,d). The SFM concentration in the bio-ink needed to be 1% (w/v) or less for reliable printing resolution.

The shear elastic and loss moduli (G' and G'') were monitored by in situ photorheometry to analyze the gelation kinetics of bio-ink solution and optimize the curing time (Figure S2). As soon as light was applied, G' of the precursor solution rapidly increased and reached the plateau. This demonstrated that the gelation process occurred very quickly and was completed within 1 min. The same behavior was observed with bio-ink solution containing SFM.

The effect of melanin contents on side gelation was evaluated by comparing the printed features with the intended features of 200−1200 μm. The addition of 1.0% (w/v) SFM to the precursor solution increased the printing resolution significantly. The printed features showed a narrow-edged shape as the concentration of melanin increased (Figure 4a,b). A precursor solution containing 1.0% (w/v) SFM with 0.2% (w/v) melanin was printable for features with a high correlation to the intended size (Figure 4b).

To evaluate the effect of melanin on the printing accuracy in the x- and y-axes, different sizes of features were printed with inks consisting of PEG4A and SFM. Figure 4c shows the comprehensive effect of SFM on printing accuracy. The

DOI: 10.1021/acsami.8b05963
ACS Appl. Mater. Interfaces 2018, 10, 23573−23582

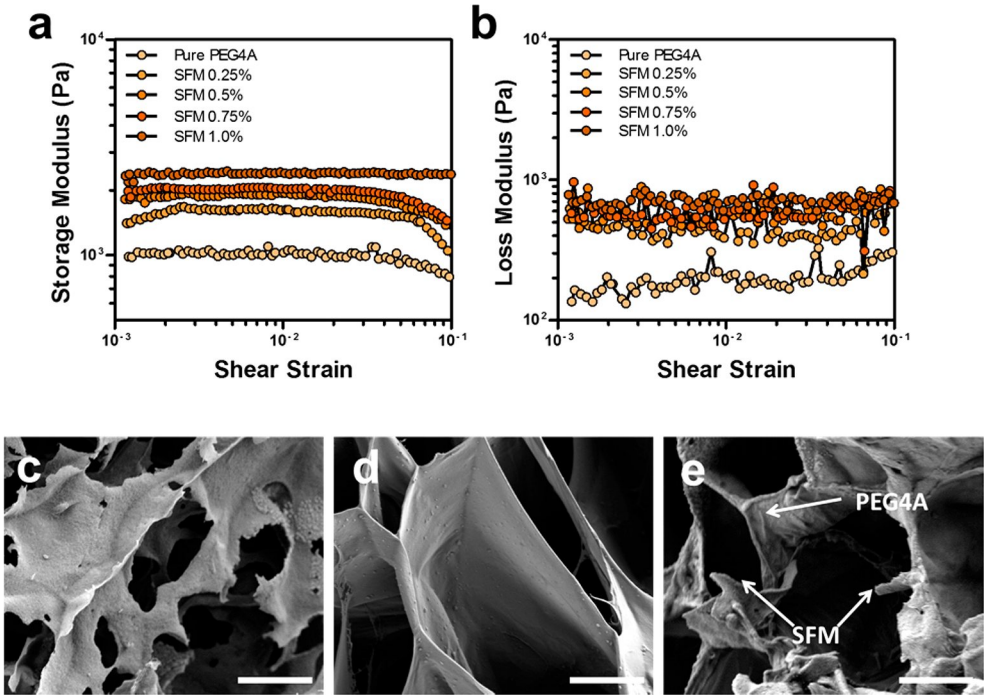

Figure 6. Effect of SFM on shear moduli of 3D-printed hydrogels. (a) Storage modulus (G') and (b) loss modulus (G'') of printed hydrogels at different concentrations of SFM in PEG4A/SFM precursor solutions. Topological images of (c) SFM, (d) PEG4A hydrogel, and (e) PEG4A/SFM hydrogel. Scale bars are 5 μm in panels c–e.

mapping of planar resolution (x- and y-axes) was expressed with black and white contrast squares based on the optical microscopic images of printed hydrogels. The brightest square indicated the lowest planar resolution with an almost 1000 μm difference from the intended feature size, while the darkest square meant a highest planar resolution with less than 1 μm difference. The addition of SF would reduce the penetration of light through the precursor solution, but unintended gelation was induced outside of the designated region due to light scattering at the surface of the SF hydrogels (Figure 4c). However, light scattering was suppressed by the addition of SFM. The melanin bound to SF effectively absorbed light and inhibited light scattering from the particle surface. The increase in melanin concentration enhanced the planar printing resolution gradually, and the size difference between the measured and the intended features was less than 1 μm at a melanin concentration of 0.2 wt %, regardless of SFM concentrations.

In printing 3D structures, the z-axis resolution is as important as the x-axis and y-axis resolution. The unique printing resolution on the z-axis is the result of cross-linking between PEG4A molecules in the path of the light beam, whose thickness is dependent on the effective penetration depth. To evaluate the printing resolution on the z-axis, the printing inks with 1 cm height were irradiated for 2 min, and the thickness of the printed hydrogel was measured. Transparent PEG4A allowed the visible range of light to penetrate freely through the ink solution, and the z-axis resolution could not be determined. Despite the light scattering by the SF hydrogels, the PEG4A/SF precursor solution without melanin also showed the deep penetration of light, forming an entire vertical range of cross-linking. In contrast, the addition of SFM to the precursor solutions significantly enhanced the printing resolution on the z-axis (Figure 4d). This gradually reduced the printing thickness, and the printing resolution was enhanced effectively.

A mesh structure of PEG4A/SFM was fabricated using vertically and horizontally aligned lines, as shown in Figure 5a. It was suggested that scaffolds with internal space were more biocompatible in tissue engineering (in terms of cell retention and viability) than bulk-type scaffolds. Lines with 500 μm width and 1 cm length were printed vertically in odd-numbered layers and horizontally in even-numbered layers. The z-motorized platform was immersed in the PEG4A/SFM precursor solution and was selectively exposed to a focused visible light beam. The irradiated regions of the PEG4A/SFM precursor solution were cross-linked, whereas nonirradiated regions remained in a liquid phase. The printed structures were washed with PBS to remove non-cross-linked precursor solutions, and porous hydrogel structures were formed (Figure 5b,c). The porous structure was observed in the optical microscopic images of the printed hydrogel structures, and the line width of the printed structures was determined to be 500 μm, as designed (Figure 5c).

The mimicry of native tissues or organs in hollow structures is extremely difficult using DLP 3D printing. PEG4A/SFM enabled the printing of blood vessel structures, as shown in Figure 5d. Briefly, 4 wt % PEG4A with 1.0 wt % SFM (0.2 wt % melanin) was used as an ink solution, and the layer height and beam irradiation time were 200 μm and 2 min, respectively. The blood vessel structure was simply printed, according to the design (Figure 5d,e). A tubular structure was observed to function as a fluidic channel (Figure 5f).

The behavior of fluids through the printed 3D vessel models were investigated at the different perfusion rates using fluorescent microscopy (Figure 5g). The PIV analysis confirmed that the velocity of the fluid varied according to the injection rate of fluorescent particles. The velocity of the fluorescent particles inside the vessel increased proportionally

DOI: 10.1021/acsami.8b05963
ACS Appl. Mater. Interfaces 2018, 10, 23573–23582

to the external injection rate of the fluid showing a stable laminar flow without leakage (Figure 5h).

The addition of SFM to precursor solutions not only improved printing resolution but also affected the mechanical properties of the printed hydrogel structures. Panels a and b of Figure 6 show the change in the shear moduli of printed hydrogels with the addition of SFM. The hydrogel photo-cross-linked with neat PEG4A showed a storage modulus of approximately 1000 Pa. When 0.2 wt % melanin was added to the same precursor solution, no significant effect on the storage modulus of PEG4A hydrogel was observed. Meanwhile, the storage modulus of the PEG4A hydrogel increased gradually with the addition of SFM, as observed with the addition of SF. SFM can be applied as a biocompatible and bioactive optical property modifier in the transparent bio-inks. Especially, it is possible to print tubular structures such as blood vessels which are impossible to be printed with a transparent ink in 3D stereolithography. The dynamic storage moduli of SFM/PEG4A hydrogels are around 10^3–10^4 Pa, commonly used for smooth muscle cells (SMC) and fibroblast cells encapsulation which constitute blood vessels.[38] In addition, it has appropriate dynamic storage moduli for adhesion and proliferation of endothelial cells.[39,40]

The surface morphology of the hydrogel structures was observed using FE-SEM. Typically, the SF aqueous solution easily changes from a random coil structure to a β-sheet structure to form a hydrogel with an interconnected structure through physical cross-linking. A cross-sectional image of the lyophilized 1% SFM hydrogel also exhibited a similar porous structure to that of the SF hydrogel (Figure 6c). Since 99% of the water occupying the solution was removed through lyophilization, a highly porous structure of SFM hydrogel was formed. The hydrogel prepared with 4 wt % PEG4A precursor solution also exhibited a porous but denser structure compared to the SFM hydrogel (Figure 6d). From the SEM images of PEG4A hydrogel containing 1 wt % SFM, the structures of SF were observed at the PEG4A hydrogel surface, confirming that SF was mixed well with PEG4A and formed a composite structure (Figure 6e). This enhanced the mechanical strength of the PEG4A/SFM composite hydrogel, because the crystalline SFM structure served as a reinforcing frame within the PEG4A hydrogel.

To investigate the biocompatibility and bioactivity of the PEG4A/SFM composite hydrogel, the cylindrical hydrogel structures carrying NIH 3T3 cells were printed, and the cell proliferation rates were evaluated using an alamarBlue assay for 13 days. The cell proliferation rate of the PEG4A/SF and PEG4A/SFM hydrogels was compared to the neat PEG4A hydrogel (Figure 7a). SF is a natural polymer used in the biological scaffolds, with advantages of biodegradability, non-cytotoxicity, and low inflammatory response. The continuous increase in cell proliferation with PEG4A/SF hydrogel resulted from SF molecules containing bioactive moieties. This continuous increase in cell proliferation was shown with PEG4A/SFM hydrogel, because the melanin was not toxic to cells. Compared with the PEG4A/SF hydrogel, the PEG4A/SFM hydrogel maintained metabolic activity similar to that of the PEG4A/SF hydrogel, which suggested that the adsorbed melanin was not toxic to NIH 3T3 cells (Figure 7a). The level of cell proliferation with PEG4A/SF and PEG4A/SFM hydrogels was higher than in neat PEG4A hydrogel after cell culture for 4 days. The difference in the cell proliferation rate between the PEG4A/SFM and PEG4A hydrogels gradually

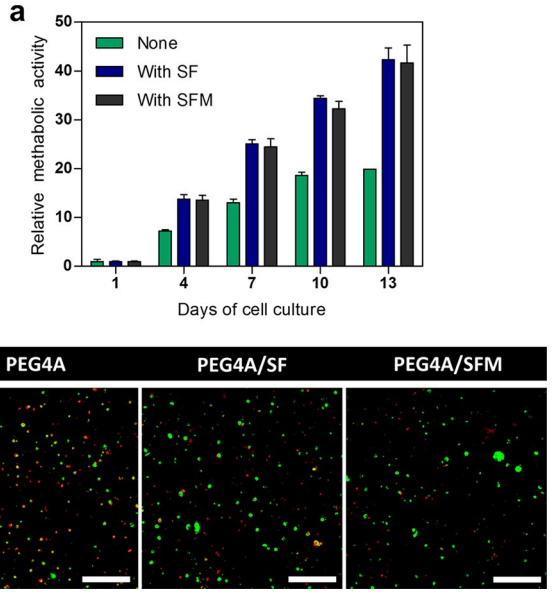

Figure 7. Biocompatibility of PEG4A/SFM hydrogels embedding cells. (a) Relative metabolic activity of NIH 3T3 cells embedded in PEG4A, PEG4A/SF, and PEG4A/SFM hydrogels after culture for 1, 4, 7, 10, and 13 days. (b) Live and dead assay of fibroblast cells embedded in PEG4A, PEG4A/SF, and PEG4A/SFM hydrogels after culture for 20 days. Scale bars are 200 μm in panel b.

increased. Furthermore, the cell proliferation of the PEG4A hydrogel was slowed by the constant metabolic activation value after cell culture for 10 days. In contrast, the PEG4A/SF and PEG4A/SFM showed a continuous increase in cell proliferation, even after longer cell culture for 13 days.

The hydrogels incubated with NIH 3T3 cells for 20 days were subjected to live and dead staining and observed using confocal laser scanning microscopy. As shown in Figure 7b, a number of dead cells were observed with PEG4A hydrogel, but more cells were alive, with PEG4A/SF and PEG4A/SFM hydrogels. PEG4A/SF and PEG4A/SFM provided a more porous structure and rough morphology, which enhanced cell attachment and survival. The higher cell density in PEG4A/SFM was consistent with the metabolic activity in Figure 7a and confirmed the biocompatibility of PEG4A/SFM as a bio-ink.

The distribution of the cells in the precursor solution was investigated by optical sectioning with a fluorescence microscope. The fluorescent signals from the cells were collected with a 100 μm depth spacing (Figure S3). The pure PEG4A bio-ink showed that most of the cells were located at the bottom of the printing bath during 3D printing layer by layer. However, it was observed that the cells were uniformly dispersed in the 3D-printed hydrogel in the bio-ink containing SFM. The addition of SFM to the bio-ink increased the viscosity of the solution and retarded the sedimentation of cells.

4. CONCLUSIONS

The development of photo-cross-linkable bio-inks is critical for the rapid 3D printing of cell-embedding structures. In particular, the transparent photo-cross-linkable polymers including acrylated PEG could not express the hollow structures, and the addition of light absorbing molecules was necessary. The addition of melanin-containing silk fibroin to

DOI: 10.1021/acsami.8b05963
ACS Appl. Mater. Interfaces 2018, 10, 23573–23582

PEG4A satisfied the requirement, and highly resolved hydrogel structures were successfully 3D-printed. The high printing resolution was achieved by restricting the light scattering of suspended SF with black melanin bound to the surface. The 3D-printing resolution was controlled through the variable addition of SFM with varying melanin concentrations. The addition of SFM to the transparent PEG4A precursor solution enhanced the printing resolution along the *x*-, *y*-, and *z*-axes significantly, as well as the mechanical stability of the printed structures. Furthermore, the PEG4A/SFM precursor solution enabled the direct printing of fluidic channels applicable to complex blood vessel networks. The printed PEG4A/SFM hydrogel structures embedding the cells proved to be non-cytotoxic and biocompatible. PEG4A/SFM hydrogels showed a higher level of cell proliferation and live cell density than PEG4A. The biocompatible SFM particles described in the research can be proposed as a generic material for the 3D printing of bio-organs and scaffolds with high resolution in the future.

■ ASSOCIATED CONTENT

Supporting Information

The Supporting Information is available free of charge on the ACS Publications website at DOI: 10.1021/acsami.8b05963.

Rheological properties of bio-inks and the effect of solution viscosity on printability; rheological behavior of PEG4A bio-inks by in situ photorheometry; sectional fluorescence images of 3D-printed hydrogels containing cells (PDF)

■ AUTHOR INFORMATION

Corresponding Author

*E-mail: jhyun@snu.ac.kr.

ORCID

Jinho Hyun: 0000-0002-9992-5681

Notes

The authors declare no competing financial interest.

■ ACKNOWLEDGMENTS

This work was supported by the Korea Institute of Planning and Evaluation for Technology in Food, Agriculture, Forestry and Fisheries (IPET) through the Agri-Bio Industry Technology Development Program funded by the Ministry of Agriculture, Food and Rural Affairs (MAFRA) (grant number 116077-03-3-HD020).

■ REFERENCES

(1) Kankala, R. K.; Zhu, K.; Li, J.; Wang, C. S.; Wang, S. B.; Chen, A. Z. Fabrication of arbitrary 3D components in cardiac surgery: from macro-, micro-to nanoscale. *Biofabrication* **2017**, *9* (3), 032002.

(2) Kankala, R. K.; Zhu, K.; Sun, X. N.; Liu, C. G.; Wang, S. B.; Chen, A. Z. Cardiac Tissue Engineering on the Nanoscale. *ACS Biomater. Sci. Eng.* **2018**, *4* (3), 800−818.

(3) Kang, H. W.; Lee, S. J.; Ko, I. K.; Kengla, C.; Yoo, J. J.; Atala, A. A 3D bioprinting system to produce human-scale tissue constructs with structural integrity. *Nat. Biotechnol.* **2016**, *34* (3), 312−322.

(4) Murphy, S. V.; Atala, A. 3D bioprinting of tissues and organs. *Nat. Biotechnol.* **2014**, *32* (8), 773−785.

(5) Grogan, S. P.; Chung, P. H.; Soman, P.; Chen, P.; Lotz, M. K.; Chen, S. C.; D'Lima, D. D. Digital micromirror device projection printing system for meniscus tissue engineering. *Acta Biomater.* **2013**, *9* (7), 7218−7226.

(6) Seck, T. M.; Melchels, F. P. W.; Feijen, J.; Grijpma, D. W. Designed biodegradable hydrogel structures prepared by stereolithography using poly(ethylene glycol)/poly(D,L-lactide)-based resins. *J. Controlled Release* **2010**, *148* (1), 34−41.

(7) Cukierman, E.; Pankov, R.; Stevens, D. R.; Yamada, K. M. Taking cell-matrix adhesions to the third dimension. *Science* **2001**, *294* (5547), 1708−1712.

(8) Elomaa, L.; Pan, C. C.; Shanjani, Y.; Malkovskiy, A.; Seppala, J. V.; Yang, Y. Z. Three-dimensional fabrication of cell-laden biodegradable poly(ethylene glycol-co-depsipeptide) hydrogels by visible light stereolithographye. *J. Mater. Chem. B* **2015**, *3* (42), 8348−8358.

(9) Ouyang, L. L.; Highley, C. B.; Sun, W.; Burdick, J. A. A Generalizable Strategy for the 3D Bioprinting of Hydrogels from Nonviscous Photo-crosslinkable Inks. *Adv. Mater.* **2017**, *29* (8), 1604983.

(10) Billiet, T.; Gevaert, E.; De Schryver, T.; Cornelissen, M.; Dubruel, P. The 3D printing of gelatin methacrylamide cell-laden tissue-engineered constructs with high cell viability. *Biomaterials* **2014**, *35* (1), 49−62.

(11) Rutz, A. L.; Hyland, K. E.; Jakus, A. E.; Burghardt, W. R.; Shah, R. N. A Multimaterial Bioink Method for 3D Printing Tunable, Cell-Compatible Hydrogels. *Adv. Mater.* **2015**, *27* (9), 1607−1614.

(12) Melchels, F. P. W.; Feijen, J.; Grijpma, D. W. A review on stereolithography and its applications in biomedical engineering. *Biomaterials* **2010**, *31* (24), 6121−6130.

(13) Lin, H.; Zhang, D. N.; Alexander, P. G.; Yang, G.; Tan, J.; Cheng, A. W. M.; Tuan, R. S. Application of visible light-based projection stereolithography for live cell-scaffold fabrication with designed architecture. *Biomaterials* **2013**, *34* (2), 331−339.

(14) Gauvin, R.; Chen, Y. C.; Lee, J. W.; Soman, P.; Zorlutuna, P.; Nichol, J. W.; Bae, H.; Chen, S. C.; Khademhosseini, A. Microfabrication of complex porous tissue engineering scaffolds using 3D projection stereolithography. *Biomaterials* **2012**, *33* (15), 3824−3834.

(15) Zhang, A. P.; Qu, X.; Soman, P.; Hribar, K. C.; Lee, J. W.; Chen, S. C.; He, S. L. Rapid Fabrication of Complex 3D Extracellular Microenvironments by Dynamic Optical Projection Stereolithography. *Adv. Mater.* **2012**, *24* (31), 4266−4270.

(16) Urrios, A.; Parra-Cabrera, C.; Bhattacharjee, N.; Gonzalez-Suarez, A. M.; Rigat-Brugarolas, L. G.; Nallapatti, U.; Samitier, J.; DeForest, C. A.; Posas, F.; Garcia-Cordero, J. L.; Folch, A. 3D-printing of transparent bio-microfluidic devices in PEG-DA. *Lab Chip* **2016**, *16* (12), 2287−2294.

(17) Bettinger, C. J.; Bruggeman, P. P.; Misra, A.; Borenstein, J. T.; Langer, R. Biocompatibility of biodegradable semiconducting melanin films for nerve tissue engineering. *Biomaterials* **2009**, *30* (17), 3050−3057.

(18) Watt, A. A. R.; Bothma, J. P.; Meredith, P. The supramolecular structure of melanin. *Soft Matter* **2009**, *5* (19), 3754−3760.

(19) Shin, S. R.; Jung, S. M.; Zalabany, M.; Kim, K.; Zorlutuna, P.; Kim, S. B.; Nikkhah, M.; Khabiry, M.; Azize, M.; Kong, J.; Wan, K. T.; Palacios, T.; Dokmeci, M. R.; Bae, H.; Tang, X. W.; Khademhosseini, A. Carbon-Nanotube-Embedded Hydrogel Sheets for Engineering Cardiac Constructs and Bioactuators. *ACS Nano* **2013**, *7* (3), 2369−2380.

(20) Shin, S. R.; Bae, H.; Cha, J. M.; Mun, J. Y.; Chen, Y. C.; Tekin, H.; Shin, H.; Farshchi, S.; Dokmeci, M. R.; Tang, S.; Khademhosseini, A. Carbon Nanotube Reinforced Hybrid Microgels as Scaffold Materials for Cell Encapsulation. *ACS Nano* **2012**, *6* (1), 362−372.

(21) Sontjens, S. H. M.; Nettles, D. L.; Carnahan, M. A.; Setton, L. A.; Grinstaff, M. W. Biodendrimer-based hydrogel scaffolds for cartilage tissue repair. *Biomacromolecules* **2006**, *7* (1), 310−316.

(22) Gillies, E. R.; Frechet, J. M. J. Dendrimers and dendritic polymers in drug delivery. *Drug Discovery Today* **2005**, *10* (1), 35−43.

(23) Hench, L. L.; Polak, J. M. Third-generation biomedical materials. *Science* **2002**, *295* (5557), 1014−1017.

(24) Gaharwar, A. K.; Dammu, S. A.; Canter, J. M.; Wu, C. J.; Schmidt, G. Highly Extensible, Tough, and Elastomeric Nano-

DOI: 10.1021/acsami.8b05963
ACS Appl. Mater. Interfaces 2018, 10, 23573−23582

composite Hydrogels from Poly(ethylene glycol) and Hydroxyapatite Nanoparticles. *Biomacromolecules* **2011**, *12* (5), 1641−1650.
(25) Gaharwar, A. K.; Rivera, C. P.; Wu, C. J.; Schmidt, G. Transparent, elastomeric and tough hydrogels from poly(ethylene glycol) and silicate nanoparticles. *Acta Biomater.* **2011**, *7* (12), 4139−4148.
(26) Pasqui, D.; Atrei, A.; Giani, G.; De Cagna, M.; Barbucci, R. Metal oxide nanoparticles as cross-linkers in polymeric hybrid hydrogels. *Mater. Lett.* **2011**, *65* (2), 392−395.
(27) Dvir, T.; Timko, B. P.; Brigham, M. D.; Naik, S. R.; Karajanagi, S. S.; Levy, O.; Jin, H. W.; Parker, K. K.; Langer, R.; Kohane, D. S. Nanowired three-dimensional cardiac patches. *Nat. Nanotechnol.* **2011**, *6* (11), 720−725.
(28) Horan, R. L.; Antle, K.; Collette, A. L.; Wang, Y.; Huang, J.; Moreau, J. E.; Volloch, V.; Kaplan, D. L.; Altman, G. H. In vitro degradation of silk fibroin. *Biomaterials* **2005**, *26* (17), 3385−3393.
(29) Wang, Y.; Rudym, D. D.; Walsh, A.; Abrahamsen, L.; Kim, H. J.; Kim, H. S.; Kirker-Head, C.; Kaplan, D. L. In vivo degradation of three-dimensional silk fibroin scaffolds. *Biomaterials* **2008**, *29* (24−25), 3415−3428.
(30) Kim, U. J.; Park, J.; Kim, H. J.; Wada, M.; Kaplan, D. L. Three-dimensional aqueous-derived biomaterial scaffolds from silk fibroin. *Biomaterials* **2005**, *26* (15), 2775−2785.
(31) Kundu, B.; Kurland, N. E.; Bano, S.; Patra, C.; Engel, F. B.; Yadavalli, V. K.; Kundu, S. C. Silk proteins for biomedical applications: Bioengineering perspectives. *Prog. Polym. Sci.* **2014**, *39* (2), 251−267.
(32) Kapoor, S.; Kundu, S. C. Silk protein-based hydrogels: Promising advanced materials for biomedical applications. *Acta Biomater.* **2016**, *31*, 17−32.
(33) Davis, N. E.; Beenken-Rothkopf, L. N.; Mirsoian, A.; Kojic, N.; Kaplan, D. L.; Barron, A. E.; Fontaine, M. J. Enhanced function of pancreatic islets co-encapsulated with ECM proteins and mesenchymal stromal cells in a silk hydrogel. *Biomaterials* **2012**, *33* (28), 6691−6697.
(34) Chen, B. Q.; Kankala, R. K.; Chen, A. Z.; Yang, D. Z.; Cheng, X. X.; Jiang, N. N.; Zhu, K.; Wang, S. B. Investigation of silk fibroin nanoparticle-decorated poly(L-lactic acid) composite scaffolds for osteoblast growth and differentiation. *Int. J. Nanomed.* **2017**, *12*, 1877−1890.
(35) Rockwood, D. N.; Preda, R. C.; Yucel, T.; Wang, X. Q.; Lovett, M. L.; Kaplan, D. L. Materials fabrication from Bombyx mori silk fibroin. *Nat. Protoc.* **2011**, *6* (10), 1612−1631.
(36) Wang, X. Q.; Kluge, J. A.; Leisk, G. G.; Kaplan, D. L. Sonication-induced gelation of silk fibroin for cell encapsulation. *Biomaterials* **2008**, *29* (8), 1054−1064.
(37) Hu, X. A.; Lu, Q. A.; Sun, L.; Cebe, P.; Wang, X. Q.; Zhang, X. H.; Kaplan, D. L. Biomaterials from Ultrasonication-Induced Silk Fibroin-Hyaluronic Acid Hydrogels. *Biomacromolecules* **2010**, *11* (11), 3178−3188.
(38) Liu, Y. X.; Chan-Park, M. B. Hydrogel based on interpenetrating polymer networks of dextran and gelatin for vascular tissue engineering. *Biomaterials* **2009**, *30* (2), 196−207.
(39) Mason, B. N.; Starchenko, A.; Williams, R. M.; Bonassar, L. J.; Reinhart-King, C. A. Tuning three-dimensional collagen matrix stiffness independently of collagen concentration modulates endothelial cell behavior. *Acta Biomater.* **2013**, *9* (1), 4635−4644.
(40) Jalali, S.; Tafazzoli-Shadpour, M.; Haghighipour, N.; Omidvar, R.; Safshekan, F. Regulation of Endothelial Cell Adherence and Elastic Modulus by Substrate Stiffness. *Cell Commun. Adhes.* **2015**, *22* (2−6), 79−89.

DOI: 10.1021/acsami.8b05963
ACS Appl. Mater. Interfaces 2018, 10, 23573−23582